

## ON THE PHYSICS OF VORTEX GENERATORS FOR FLOW SEPARATION CONTROL

Benoît Gardarin and Laurent Jacquin

Dept of Fundamental and Experimental Aerodynamics ,  
Onera - DAFE  
8, rue des Vertugadins, 92190 Meudon, FRANCE  
benoit.gardarin@onera.fr

### ABSTRACT

We aim at analyzing the physical phenomena fixing the global efficiency of Vortex Generators for turbulent flow separation control. Fluidic and Mechanical Vortex Generators characteristic are considered. The vortices properties are evaluated with mean of hot wire and PIV measurements. We show that two mechanisms are likely participating in fixing the control strategy efficiency. The first one is mixing, carried out by vortices. The second one is an instability mechanism, which is responsible for the vortex system disruption. An efficient control strategy thus results from a compromise between improving vortex mixing and delaying the development of vortex instability.

### INTRODUCTION

Mechanical or fluidic vortex generators (VGs) are now genuinely used in several applications. For instance, these systems have proved to be efficient in delaying massive flow separations which occur above wings/blades or at the inlet of air intakes when some critical angle of attack is reached, or when strong duct curvatures cannot be avoided. Many empirical studies dealing with vortex generators for separation control have been conducted in order to define optimal configurations of VGs given flow parameters, see Lin(2002), Jenkins (2002). However, the mechanisms fixing their efficiency of a VGs arrangement are not yet really understood. The present study aims at providing physical insights into this topic by exploring the role of vortex dynamics and its possible contribution in setting a limit to the efficiency of such systems. An experiment has been conducted on the particular case of a channel diffuser in which flow separation occurs on a rounded ramp. Mechanical Vortex Generators (MVGs) and Fluidic Vortex Generators (FVGs) have been tested. The vortices produced by these VG systems and the flow modifications to which they lead are surveyed using smoke and wall flow visualizations, hot wire anemometry and PIV. In particular, different parameters which characterize the dynamics of the vortices (core radius, circulation, Reynolds stresses and spectra) are determined. The unsteady properties of the different vortex arrangements produced by the VGs are discussed, especially in relation with hydrodynamic stability theory. Gardarin *et al* (2007) have shown that instability mechanisms are at work and are likely fixing one of the bounds of VGs efficiency. Vortex systems produced by our MVGs and FVGs being quite different (number of vortices, individual circulation), their comparison provides new insights into the physics of these control devices. This allows to better delineate the limits of this conventional control approach.

### EXPERIMENTAL SETUP

The present experiments were conducted in the S19 wind tunnel of Onera-DAFE which has been conceived to investigate flow separation induced by a backward facing ramp, see Figure 1. This closed-loop tunnel has a test section of 300 mm width for 2 m long. The maximum speed of incoming flow is about  $30 \text{ ms}^{-1}$  with an associated turbulence rate of 0.2%. The lower wall is a rounded ramp of 210 mm height, while the upper one has been determined numerically in order to avoid its boundary layer separation. The transition of the channel boundary layers is triggered with a strip of *Carborandum*, located 750 mm upstream from the beginning of the test section. Flow visualizations have been made using standard techniques (DEHS smoke in the channel and oil mixture for wall flow visualisations). In its reference configuration *i.e.* without any flow control device, the freestream velocity entering the test section is set to  $30 \text{ ms}^{-1}$ , which corresponds to a Reynolds number of  $4.0 \times 10^5$  based on the ramp height. The boundary layer was measured at  $X = 0$ , and found to have a thickness  $\delta = 20 \text{ mm}$ . At  $X = 5\delta$ , the boundary layer separates before reattaching near  $X = 29\delta$  in the symmetry plane  $Y = 0$ . Velocity measurements have been performed with Stereo Particle Image Velocimetry in both  $YOZ$  and  $XOZ$  vertical planes, using DANTEC Software Dynamic Studio. The light source is produced by a Quantel double cavity ND-YAG laser of  $120 \text{ mJ/pulse}$  of 532 nm wavelength. The light sheet thickness has been adjusted to 2 mm. Each camera uses a CCD sensor of  $2048 \times 2048$  pixels, and is equipped with a Scheimpflug mechanism. The instantaneous images were processed using  $32 \text{ pixels} \times 32 \text{ pixels}$  interrogation windows with 50% overlap, allowing interrogations windows as small as  $1.5 \text{ mm} \times 1.5 \text{ mm}$ . The acquisition rate of both laser and camera is 4 Hz. The tracers used are DEHS droplets, which diameter is nominally inferior to  $1 \mu\text{m}$ . For each measured plane, 1000 images were used so as to determine both mean and turbulent fields. The calibration method used a pinhole method, which is considered more reliable than the polynomial one (see Le Sant *et al*, 2007).

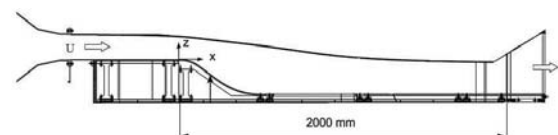


FIGURE 1 – Wind Tunnel Geometry

Velocity fluctuations spectra have been performed using a single hot wire DANTEC 55P11. The spectra have been obtained using 150 data blocks, acquired at an acquisition

rate  $f_{acq} = 12Khz$  and low-pass filtered at  $f_c = 4Khz$ .

## RESULTS AND DISCUSSION

### Flow Control

#### Mechanical Vortex Generators (MVGs).

Figure 2 shows the wall flow visualisation by oil mixture in the case of a passive control with a range of 8 counter-rotating vortex generators. They are located at  $5\delta$  upstream of the boundary layer separation line where  $\delta$  denotes the boundary layer thickness at  $X = 0$  (the origin of the coordinate frame is indicated in Figure 1). Their length and height are respectively  $1.8\delta$  and  $0.6\delta$ , the distance between two counter-rotating pairs being  $\lambda = 3.6\delta$ . Their inclination with the flow direction has been set to  $20^\circ$ .

These different geometrical parameters are close to those recommended by other authors, see Lin (2002). A preliminary parametric study, based on the wall flow visualisation, has confirmed that this choice leads to the smallest detachment area. We can see that the flow undergoes a lateral contraction, the flow reattaching in the central region and separating at the corners where secondary flows develops. The dashed lines delineates the separations.

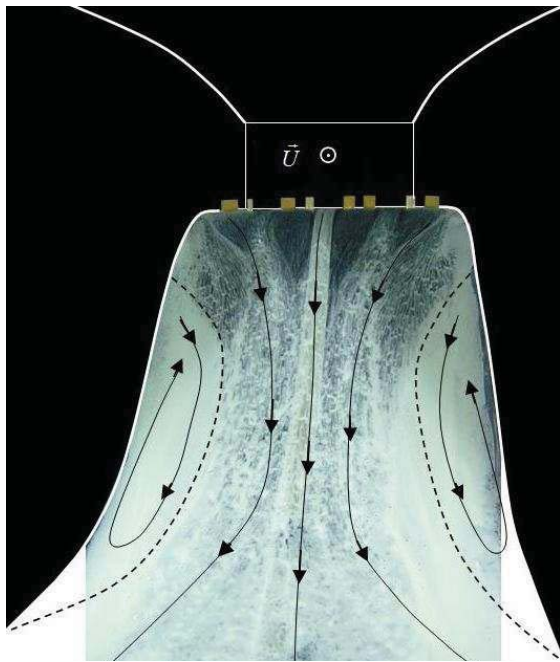


FIGURE 2 – Flow visualisation behind MVGs

#### Fluidic Vortex Generators (FVGs).

While the counter rotating configuration is the most efficient in term of separation reduction for MVGs, preliminary tests have shown that for FVGs, co-rotating cases delay the separation most efficiently than counter rotating cases. This will be discussed further below. We selected a skewed row of 18 jets making an azimuthal angle of  $30^\circ$  with the main flow, and located  $5\delta$  upstream of the boundary layer separation line. The white arrows on Figure 3 represent the jets arrangements. For clarity reasons, every second jets is displayed. Their diameter is  $0.1\delta$ , the distance between two jets being  $0.75\delta$ . Measurement of jets velocity was performed using a

sonic throat. Several injection to free-stream velocity ratio  $VR = U_i/U_0$  were investigated. For  $VR = 0$  to  $VR = 5$ , the separation length reduces and the flow reattaches in the central region for  $VR = 5$ . For  $VR \geq 7$ , the flow separates again in the middle of the channel. Measurements shows that for such high values of  $VR$ , vortices do not form anymore downstream. Thus, the best value which have been retain is  $VR = 5.5$ . The corresponding flow topology on the lower wall is close to that of MVGs. The flow remains attached in the middle of the channel, and separates on each corner. However, the separated regions, delineated by the dashed lines, are less important than for the MVGs configuration.

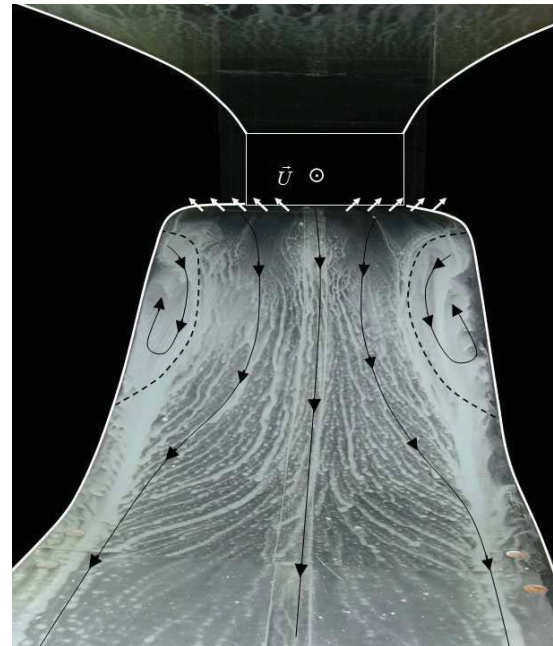


FIGURE 3 – Flow visualisation behind FVGs

### Vortex Dynamics

In this section, we aim at analyzing the dynamic of the vortices produced by the VGs as done by Gardarin *et al* (2008). In particular, MVGs and FVGs are compared. The two cases strongly differ, regarding the number of actuators (8 *versus* 18) and the signs of their trailing vorticity. The Figure 4 shows velocity profiles deduced from PIV measurements in the middle of the channel. Each controlled case is compared with the reference configuration. We can see that recirculation (negative velocity) is suppressed by the VGs in the central region. This is induced by the increase of momentum exchanges by the vortices. As a result, the boundary layer remains attached in the center of the channel.

#### Shear Stresses $\overline{v'w'}$ .

It have been shown (Gardarin *et al*, 2008) that the global efficiency of mechanical vortex generators depends on instability mechanisms which develops inside vortices. These instabilities, which develops when several vortices are put in interaction, are responsible for the vortex system disruption. One may hypothesize that those mechanism may not develop in the same way for MVGs and FVGs. A mean of investigating the presence of trailing vortices instabilities is to consider the shear stress  $\overline{v'w'}$  distribution. Indeed, cooperative instability are due to the stretching of vorticity perturbations by the strain field produced by a neighboring

vortices. As a result, the vortex core move in a privileged direction inclined about  $45^\circ$  respectively to the lower wall. This motion is superposed to a random displacement of the vortex, called *vortex meandering*. Actually, an isolated vortex is already subjected to this phenomenon whose origin is not yet fully understood (see Jacquin *et al*, 2003)

In 1996, Devenport has proposed a simple model explaining the shear stress distribution  $\overline{v'w'}$  in a vortex. Assuming that its center distribution can be modeled as a Gaussian distribution (that is modeling only the vortex meandering), he shows that the  $\overline{v'w'}$  structure is a quadripolar one, alternating positive and negative values along diagonal directions. In particular,  $\overline{v'w'}$  is nil in the vortex center. Figure 5 shows the shear stress distribution deduced from PIV measurement for MVGs and FVGs. It exhibits a quadripolar structure but it looks different : contrary to pure meandering, one gets unbalanced negative and positive poles and shear stress is not nil at the vortex centre. This indicates that the vortex displacement is not purely random and contains a coherent dynamics component.

Actually, stretching of the vortices is induced by their mirror images below the wall. This stretching direction, which is oriented about  $45^\circ$ , leads to cooperative instabilities. The shear stresses corresponding to these amplified perturbations is no longer quadripolar, but exhibits a distribution such as those shown in figure Figure 5, with, in particular,  $\overline{v'w'}(y = 0, z = 0) \neq 0$ . This results proves that, as in the MVG's configuration, the vortices of the FVGs are also subjected to cooperative instabilities.

**Cooperative Instabilities.**

If we consider the influence of the lower wall as a symmetry plane, each vortex is subject to the influence of the strain field induced by its image. It means that in the present configurations, long and short wave instabilities may occur.

The long wave instability refers to the well known Crow instability (Crow, 1970). This long wave mechanism develops for example in the wake vortex pair produced by a plane, and is responsible for its final destruction. Its wavelength is of several times the distance separating the two vortex cores. Let  $b$  denote the distance between the vortex core to its image : one gets  $kb = O(1)$  for the most amplified wavelength. The short wave instability, also called *elliptic* instability has been described by several authors, see Widnall (1974), Moore and Saffman (1975), Tsai and Widnall (1976). This short wave instability is characterized by an axial wave number  $ka = O(1)$ , meaning that the wavelength is of several times the vortex core radii. Several studies have been conducted, showing experimental evidences of the development of these mechanism in vortices.

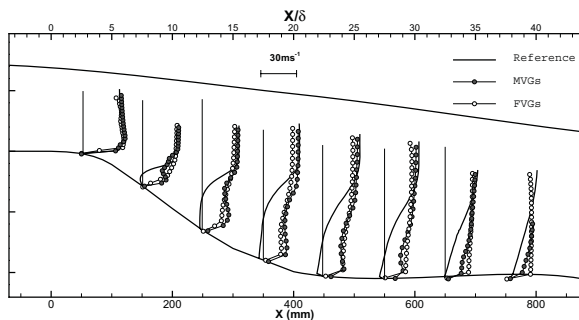


FIGURE 4 – Velocity profiles at  $Y = 0$  for the reference case, MVGs and FVGs.

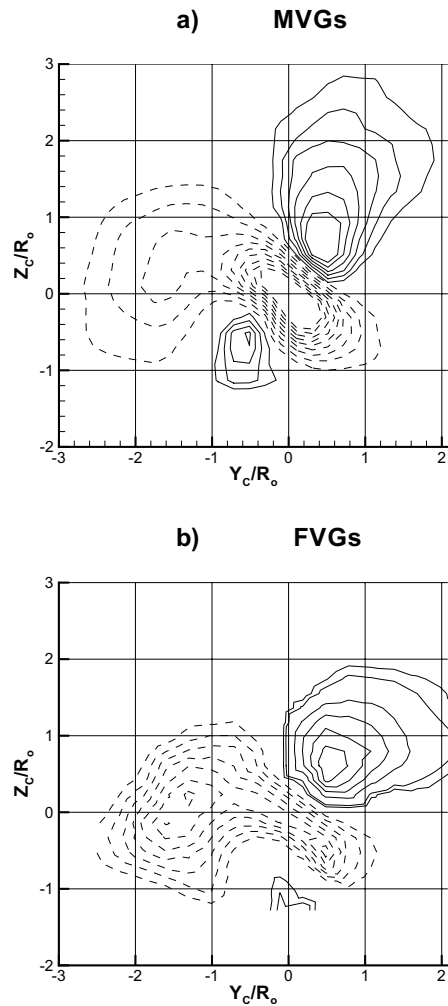


FIGURE 5 – Shears Stresses  $\overline{v'w'}$  for mechanical (a) and fluidic (b) vortex generators at  $X = 2.5\delta$ . Negative values are dashed.

For example, Leweke and Williamson (1998) have investigated the interaction of the short-wavelength instability with the long-wavelength one. More recently, an experimental study of wake instabilities has been conducted by Ortega (2003) in a counter-rotating vortex configuration. In the previous section, we have seen cooperative instabilities were at work inside vortices. A spectral analysis may provides some useful information on the type of instabilities which are at work.

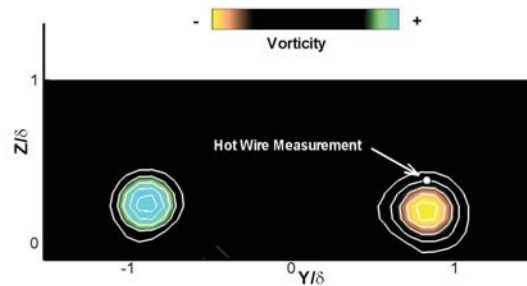


FIGURE 6 – Hot Wire location for Spectral Analysis. (MVG case at  $X = 4\delta$ )

As shown on Figure 6, we have measured each spectra away one radius of the vortex centre. This probe location turns out to be most convenient in order to discriminate the cooperatives instabilities frequencies. Figure 7 shows the resulting power spectral densities of velocity fluctuations, measured on vortices at  $X = 4\delta$ .

For the mechanical VG case, the spectra clearly exhibits two peaks. The first one, located at  $f \approx 350Hz$ , corresponding to  $kb \approx 1.1$ , is in a good agreement with the results of the Crow instability ( $kb = 1$ ). The second one, located near  $f \approx 820Hz$  is not easy to interpret and may be related to transient growths inside vortices. The FVG case exhibits a peak around  $kb = 1$  corresponding to the Crow instability. But contrary to the MVG case, no other peak is found on this spectra.

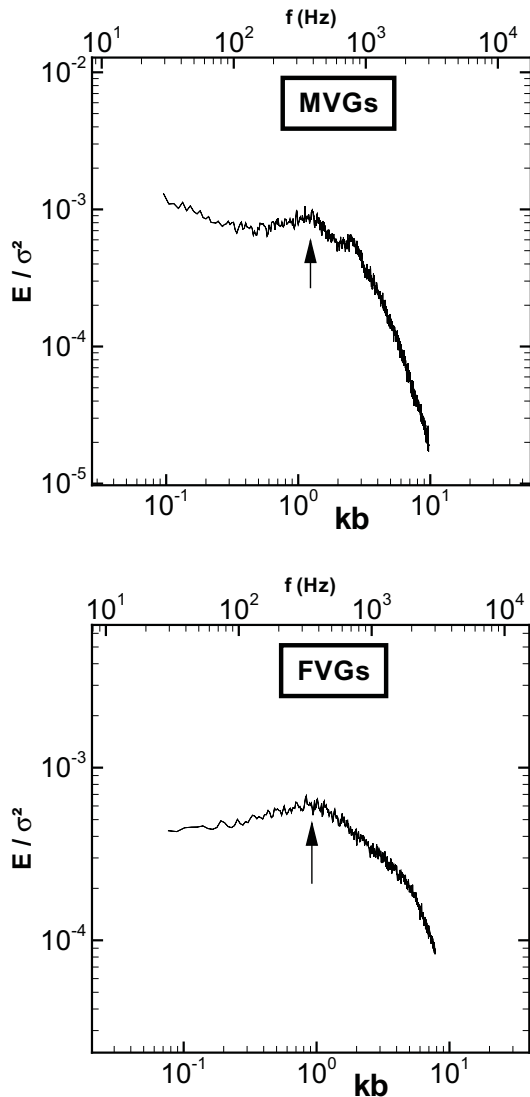


FIGURE 7 – Normalized spectral energy of the axial velocity measured with a hot-wire probe at  $X = 4\delta$  and  $r = R_0$ . Top : Vortex Coming from a Mechanical Vortex Generator. Bottom : Fluidic Vortex Generator.

Considering cooperative instability, in the case where only two vortices separated by a distance  $b$  are considered (see e.g. Sipp et al. 2003), whatever the length scale (short or long), the instability amplification rate is fixed by the shear rate :

$$\tau_i^{-1} = \frac{\Gamma}{2\pi b^2} \quad (1)$$

In this relation,  $\Gamma$  denotes the circulation which can be determined according to the following relation :

$$\Gamma = \iint_{\Omega} \omega_x(y, z) d\Omega \quad (2)$$

where  $\omega_x(y, z)$  denotes the axial vorticity, and  $\Omega$  an appropriate domain around vortices. The table 1 shows the values of  $\Gamma$ ,  $b$  and  $\tau_i^{-1}$ , determined from the PIV measurements. One can notice that the circulation of a vortex produce by MVG is nearly two times larger that produce by the FVG. The distance separating the vortex core and its image being nearly the same for the two actuators, the amplification rate  $\tau_i^{-1}$  of the cooperative instability is larger in MVG's vortex.

TABLE 1 – Vortices Characteristics for Mechanical and Fluidic case at  $X = 4\delta$ .  $N$  denotes the number of vortices.

VG Type	$N$	$\Gamma(m^2s^{-1})$	$b(10^{-3}m)$	$\tau_i^{-1}(10^2s^{-1})$
MVG	8	0.51	15	3.6
FVG	18	0.24	12	2.6

#### Vortex Mixer

Interestingly, we can point out that while the absolute circulation of the FVGs vortices is half that of the MVGs, the number of FVGs is twice that of the MVGs. Therefore, the product  $N|\Gamma|$ , where  $N$  denotes the number of vortices and  $|\Gamma|$  the absolute value of their vortex circulation, remains the same (see table 2). This product seems to play a role in selecting an efficient control. Reducing  $N$  by a factor 2 for the FVGs were inefficient in term of separation reduction. Using only three pairs of counter rotating mechanical actuators (instead of four) also results in a large separation. Consequently, a minimum value of  $N|\Gamma|$  seems to be necessary to suppress flow separation. Let  $\bar{\Gamma}$  denotes this critical value of  $N|\Gamma|$ .

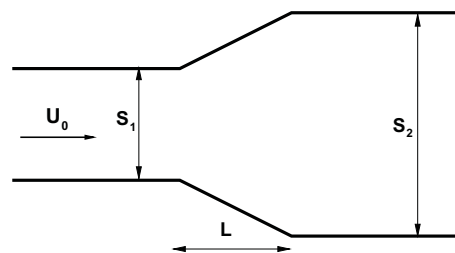


FIGURE 8 – Geometrical Parameters of a Diffuser

If we consider a model case of flow separation in a diffuser as schematized on Figure 8, two different time scales can be introduced. The first one is the convection time  $\tau_C$  it takes for the fluid to cross the length  $L$  of the diffuser. According to Figure 8, we have :

$$\tau_C = \frac{L}{U_0} \quad (3)$$

The second time scale is a mixing time  $\tau_M$ , which characterizes the time taken by vortices to mix momentum along the diffuser. Vortices are characterized by their total absolute circulation  $\bar{\Gamma}$ . Considering that these vortices are able to mix momentum so as to avoid separation in the diverging portion of the duct, that is from section  $S_1$  to section  $S_2$ , one takes for  $\tau_M$  :

$$\tau_M = \frac{S_2 - S_1}{\bar{\Gamma}} = \frac{\Delta S}{\bar{\Gamma}} \quad (4)$$

Efficient control is obtained when these two time scales are comparable. This leads to the condition :

$$\frac{\tau_M}{\tau_C} = \frac{U_0 \Delta S}{\bar{\Gamma} L} \approx 1 \quad (5)$$

This proposal has been tested using our data, and the results are shown in Table 2.  $\Delta S$  is the product of the ramp height by the channel span. Whatever the nature of the VGs used (MVGs or FVGs), we have  $\tau_M/\tau_C \approx 1$  in accordance with (5). In this table, we also give the values of  $\tau_i/\tau_C$ , which characterizes the amplification of instability in the vortex system. One must have  $\tau_i/\tau_C \ll 1$ , a value of about 0.2 being known as that above which the strength of the vortex system is strongly alleviated (This is at least the case for counter-rotating vortex pairs, see Spalart (1996)). As seen in Table 2, this condition is fulfilled in our flow.

TABLE 2 – Absolute circulations and Characteristic time scales for MVGs and FVGs

VG Type	$N \Gamma (m^2s^{-1})$	$\tau_C(10^{-3}s)$	$\tau_M/\tau_C$	$\tau_i/\tau_C$
MVG	4.08	1.66	0.93	0.17
FVG	4.32	1.66	0.88	0.23

This analysis has been also tested in other cases described in the literature, see Table 3 and 4. The difficulty is the evaluation of  $\Gamma$  from these data, this quantity being rarely measured. Therefore, we restrict ourself to cases based on MVGs, and evaluate  $\Gamma$  from the lifting line theory according to the following relation :

$$\Gamma = \frac{KC_z S}{2h} U_{eq} \quad (6)$$

$S$  denotes the VG area,  $K$  is a constant taken for reasons of simplicity as  $2/\pi$  (elliptic loading),  $C_z$  the lift coefficient of the VG, and  $U_{eq}$  is an equivalent velocity which takes into account the velocity deficit into the boundary layer. With  $\delta$  the boundary layer thickness and  $h$  the MVGs height, we use :

$$U_{eq} = \frac{U_\infty}{h} \int_0^h \left(\frac{y}{\delta}\right)^{\frac{1}{7}} dy \quad (7)$$

Both (6) and (7) provide rough estimations of circulation induced by a mechanical VG. The parameters given by different authors are indicated in Table 3. The corresponding time scale ratios are shown in Table 4. These test cases cover a wide range of parameters, including a separated flow on the rear part of a bump in a transonic regime (Bur, 2008). The variations of  $\tau_M/\tau_C$  and  $\tau_i/\tau_C$  almost fulfill the conditions  $\tau_M/\tau_C \approx 1$  and  $\tau_i/\tau_C > 0.2$ .

More generally speaking, the capacity of a flow to avoid separation strongly depends on its ability to mix momentum between the outer region and the separated one. When a laminar flow is considered, this is done by the fluid viscosity  $\nu$ .

TABLE 3 – Different experiments on separation control by VGs : (1) Godart *et al* (2005); (2) Velte *et al* (2008); (3) Jenkins *et al* (2002); (4) Gardarin *et al* - MVGs, present study; (5) Gardarin *et al*- FVGs, present study; (6) Bur, (2008)

Ref	$\delta$ (mm)	$\Delta S$ (m <sup>2</sup> )	$N$	$L$ (m)	$U_o$ (ms <sup>-1</sup> )	$\Gamma$ (m <sup>2</sup> s <sup>-1</sup> )
(1)	455	0.6	4	2	10.3	0.78
(2)	25	0.018	8	0.15	1	0.014
(3)	22	0.021	14	0.34	42	0.32
(4)	20	0.063	8	0.5	30	0.5
(5)	20	0.063	18	0.5	30	0.24
(6)	4	0.0014	9	0.1	390	0.49

TABLE 4 – Characteristic time scales

Ref	$\tau_C(10^{-3}s)$	$\tau_M/\tau_C$	$\tau_i/\tau_C$
(1)	194	0.99	3.07
(2)	150	1.04	4.8
(3)	8	0.59	0.15
(4)	16.6	0.95	0.17
(5)	16.6	0.88	0.23
(6)	0.25	1.27	0.5

For a turbulent flow, the mixing may be considered as being performed by an equivalent viscosity  $\nu_t$  which is larger than  $\nu$  by several orders of magnitude. As a result, a turbulent boundary layer is more likely to resist to adverse pressure gradient than a laminar one. But when too strong pressure gradients are encountered, another mixing mechanism have to be introduced to avoid separation. This is performed by injection of the vortices produced by the VGs which “work” as an equivalent viscosity  $\nu_\Gamma = N|\Gamma|$ . At the same time, as seen in Table 4, the cooperative instability time scale  $\tau_i$  must be larger than  $\tau_C$  to avoid disruption of the vortex system.

## CONCLUSION

The possibility of controlling turbulent boundary layer separation in a channel diffuser with mean of Vortex Generators is considered. In particular, Mechanical and Fluidic VGs are examined with a vortex dynamic point of view. For each case, an efficient arrangement in term of separation reduction is selected. While efficient arrangements markedly differ when MVGs or FVGs are considered, we have shown that two mechanisms plays a major role in their selection :

- The first is mixing carried out by the vortices. The mixing capacity of the vortex system is evaluated by  $N|\Gamma|$ ,  $N$  being the number of vortices produced by the VGs and  $\Gamma$  the circulation of each individual vortex. This mechanism, characterized by its time scale  $\tau_M = \frac{\Delta S}{N\bar{\Gamma}}$ , where  $\Delta S$  is a characteristic mixing area, provides useful information on the number of actuators needed to control the flow separation.
- The second mechanism is an instability mechanism which corresponds to the development of a long wave cooperative instability on each vortex due to its mirror image. This mechanism is characterized by a time timescale  $\tau_i = \frac{2\pi b^2}{\Gamma}$ ,  $b$  being the distance between

the vortex core and its image. This instability, which finally leads to vorticity elimination, have to be delayed so has to optimized the control efficiency (see Gardarin *et al* 2008).

Given a separation  $b$ , a compromise must be found between the minimisation of  $\tau_M$ , which requires a large circulation, and the maximisation of  $\tau_i$ , which requires a weak circulation.

## REFERENCES

- Bur, R. *Private communication*, 2008
- Crow, S.C., "Stability theory for a pair of trailing vortices", *AIAA Journal*, (8), (12), pp. 2172-2179, 1970
- Devenport, J., Rife, M.C., Liapis, S. I., and Follin, G. J., "The Structure and Development of a Wing-Tip Vortex", *Journal of Fluid Mechanics*, vol. 312, pp. 67-106, 1996
- Gardarin, B., Jacquin, B. and P. Geffroy, "Flow Separation Control With Vortex Generators", *4th Flow Control Conference*, AIAA paper 2008-3773, 2008
- Godard, G. and Stanislas, M., "Control of a decelerating boundary layer. Part 1 : Optimization of passive vortex generators", *Aerospace Sciences and Technology* 10 (3), pp. 181-191, 2006
- Jacquin, L., Fabre, D., Sipp, D., Vollmers, H., and Theofilis, V., "Instability and unsteadiness of aircraft vortex wakes", *Aerospace Science and Technology*, vol 7,(8) , pp. 577-593, 2003
- Jenkins L, Gorton SA, Anders S. "Flow control device evaluation for an internal flow with an adverse pressure gradient", AIAA Paper 2002-0266, *40th AIAA Aerospace Sciences Meeting and Exhibit*, Reno, NV, January 14-17, 2002
- Ortega, J. M., Bristol R. L., Savas ., "Experimental study of the instability of unequal-strength counter-rotating vortex pairs". *Journal of Fluid Mechanics*, 474 , pp 35-84, 2003
- Y. Le Sant, B. Gardarin, B. Leclaire, P. Geffroy, D. Soulevant , "Polynomial calibration vs pinhole calibration", *7th International Symposium Particle Image Velocimetry*, Rome, Italy, September 2007
- Leweke, T., Williamson, C.H.K, "Cooperative elliptic instability of a vortex pair", *Journal of Fluid Mechanics*, vol.360, pp. 85-119, 1998
- Lin JC., " Review of research on low-profile vortex generators to control boundary-layer separation", *Progress in Aerospace Sciences*, 38 389-420, 2002
- Moore, D.W., Saffman, P.G., "The instability of a straight vortex filament in a strain field", *Proc. Roy. Soc. London Ser. (A)* 346 413-425, 1975
- Sipp D., Jacquin L. : "Widnall instabilities in vortex pairs". *Physics of Fluids*, Vol. 15, 2003
- Spalart, P. R., and Wray, A. A., "Initiation of the Crow Instability by Atmospheric Turbulence", *The Characterization and Modification of Wakes from Lifting Vehicles in Fluids*, AGARD, pp. 18.1-18.8.,1996
- Tsai, C., Widnall,S.E., "The stability of short waves on a straight vortex filament in a weak externally imposed strain field", *Journal of Fluid Mechanics*, vol. 73, pp. 721-733, 1976
- Velte C.M., M. O. L. Hansen and D Cavar, "Flow analysis of vortex generators on wing sections by stereoscopic particle image Velocimetry measurements", *Environ. Res. Lett.* 3, 2008
- Widnall, S.E., Bliss, D.B., Tsai, C. Y., "The instability of short waves in a vortex ring" , *Journal of Fluid Mechanics*, vol. 66, pp. 35-47, 1974